JOURNAL OF GEOPHYSICAL RESEARCH, VOL. 104, NO. A1, PAGES 153–163, JANUARY 1, 1999

Systematic modeling of soft-electron precipitation effects on high-latitude F region and topside ionospheric upflows

Y.-J. Su,[1] R. G. Caton,[2] J. L. Horwitz, and P. G. Richards

Center for Space Plasma and Aeronomic Research, University of Alabama in Huntsville

Abstract. An ionospheric plasma fluid transport model is used to investigate the effects of soft (<1 keV) electron precipitation on high-latitude F region/topside ionospheric O^+ upflows. In this paper we present a systematic modeling study of ionospheric effects of varying soft-electron precipitation, focusing on the resulting upward O^+ ion velocities and fluxes, as well as the elevated ion and electron temperatures, due to the precipitation. Recent satellite observations [*Seo et al.*, 1997] suggest an inverse relationship between upward O^+ fluxes and the characteristic energy of the precipitating electrons for the same energy flux level. The modeling results presented here show this inverse relationship explicitly. Our interpretation is that a declining characteristic energy at constant energy flux increases the number of precipitating electrons available to heat the thermal electrons, and thus enhances the thermal electron temperature and hence the ambipolar electric field for propelling the upward O^+ flows. The modeled increase of the thermal electron temperature with enhanced auroral electron precipitation is also generally consistent with the *Seo et al.* [1997] topside ionospheric plasma measurements. In addition, the modeling results presented here illustrate characteristic temporal development responses, showing dramatic increases in velocity, Mach number, and flux values during the first 10-13 min after the precipitation is turned on. By ~1 hour after the initiation of a soft-electron precipitation event the ion upward velocities and fluxes approach nearly stable, asymptotic values.

1. Introduction

Strong field-aligned upward flow velocities of O^+, at times approaching 1 km s^{-1}, are frequently observed at topside altitudes in the high-latitude ionosphere in both radar and satellite measurements [*Wahlund et al.*, 1992; *Ganguli et al.*, 1994; *Tsunoda et al.*, 1989; *Yeh and Foster*, 1990]. Several different processes have been suggested as possible contributing drivers of these upflows. These suggested drivers include convection-driven frictional ion heating in strong convection events [e.g., *Korosmezey et al.*, 1992; *Heelis et al.*, 1993; *Wilson*, 1994] and electron temperature enhancements [e.g., *Whitteker*, 1977], as induced by various processes including thermal electron heating by electron precipitation, for example, in the cleft region. Also, *Ganguli et al.* [1994], in examining Dynamics Explorer (DE) 2 measurements of ion convection and vertical flow velocities, regarded the simultaneous observations of ion upflows and large shears in the ion convection velocity as evidence of field-aligned upflows, which are driven mainly by ion heating due to Kelvin-Helmholtz-type instabilities.

Richards [1995] modeled effects on the F region electron density and temperature of a soft auroral electron precipitation event. Recently, there have been detailed comparisons between fluid models and both radar and satellite data for the effects of soft-electron precipitation on high-latitude F region/topside ionospheric upflows. *Liu et al.* [1995] successfully modeled both HILAT and DE 2 ionospheric thermal ion and electron characteristics at auroral latitudes using an ionospheric fluid plasma transport model with the spacecraft-measured ion convection velocities and soft-electron precipitation characteristics as inputs. *Caton et al.* [1996] simulated three profiles of density, temperature, and flow velocity obtained with the European Incoherent Scatter Radar (EISCAT) using the same ionospheric plasma transport code used by *Liu et al.* [1995]. The results of *Caton et al.* [1996] indicated a dominant role for soft-electron precipitation as well as downward magnetospheric heat fluxes in driving these EISCAT-observed F region/topside ionospheric upflows.

[1]Now at Space and Atmospheric Sciences, Los Alamos National Laboratory, Los Alamos, New Mexico.

[2]Now at Radex Inc., Bedford, Massachusetts.

Paper number 1998JA900068.
0148-0227/99/1998JA900068$09.00

The purpose of this paper is to analyze the effects of soft-electron precipitation in driving ionospheric upflows using a systematic modeling approach. This is accomplished by varying only the soft-electron precipitation characteristics (characteristic energy, energy flux, and number flux), while leaving all other independent ionospheric and neutral atmospheric parameters fixed, to examine the consequent effects on the ionospheric density, temperature, and velocity parameters in the altitude range of 200-1000 km. In order to elucidate the temporal development of upflows subject to such precipitation we have also examined the characteristic ionospheric dynamic response to a gradual onset of the precipitation. *Heelis et al.* [1993] have performed an investigation of the differences in field-aligned flows driven by frictional ion heating in abrupt and gradual subauroral ion drift (SAID) events. Their results suggest that a much larger upward flow results when the maximum SAID convection speed is instantaneously applied (within a 15-s time step) rather than when the SAID speed is gradually increased over 5-10 min.

2. Ionospheric Dynamics Model

In modeling the high-latitude F region/topside ionospheric dynamics here, we used the field line interhemispheric plasma (FLIP) model described by *Richards and Torr* [1986], *Liu et al.* [1995], and *Caton et al.* [1996]. The basic code is the time-dependent one-dimensional model along a closed dipolar flux tube from 80 km in the Northern Hemisphere to 80 km altitude in the Southern Hemisphere. A tilted dipole approximation is used for the Earth's magnetic field. After the field line grid, neutral atmosphere densities and temperatures, and photoproduction rates have been established, the solution of the transport equations proceeds in the following order. First, the photoelectron transport equations are solved to provide electron heating rates and secondary ion production rates. Second, the energies are solved to provide ion and electron temperatures. The continuity and momentum equations are solved to obtain the major ion densities (O^+ and H^+). Finally, the minor ion equations are solved to obtain densities for N^+ and He^+. In this paper the only change from the situation in the work by *Caton et al.* [1996] is that the soft-electron precipitation allowed to linearly ramp to its maximum value over a period of time rather than the abrupt turn-on used by *Caton et al.* [1996]. The electron precipitation is described through a designation of a characteristic energy and a total energy flux in a two-stream auroral electron model [*Richards and Torr*, 1990]. The mass spectrometer and incoherent scatter (MSIS-86) model [*Hedin*, 1987] is used for the neutral densities and temperatures in this paper. The HWM90 model [*Hedin et al.*, 1991] is used for the neutral wind. The model was run for a flux tube located at 69° geographic latitude and 19° geographic longitude on February 20, 1990. This is representative of the EISCAT radar site at which significant ionospheric upflows are frequently observed [e.g., *Wahlund et al.*, 1992; *Caton et al.*, 1996].

For each set of results an initial run with no precipitation of 24 hours was first completed, thereby allowing equilibrium to be reached before the precipitation was initiated. Then, starting with that baseline condition, several simulations with precipitation events ranging in duration from 30 min to 2 hours were carried for various precipitation electron energy flux and characteristic energy levels. We then utilized this information to for distilled parameter relationship plots to portray the systematic effects of the soft-electron precipitation parameters on the resulting upflow characteristics. For the runs whose results are presented here the precipitation was initiated at 2130 UT, which corresponds to late evening at 2204 LT, to reduce the possible obscuration by additional photoionization effects. The range of characteristic precipitating electron energies chosen was 50-600 eV, while the energy flux was varied from 0.5 ergs cm^{-2} s^{-1} to 6.0 ergs cm^{-2} s^{-1}. These values are within the ranges measured by the Low Altitude Plasma Instrument (LAPI) on board DE 2 [*Winningham et al.*, 1981]. In order to focus only on the systematics of soft-electron precipitation the possible frictional ion heating stemming from ion convection through the neutral gas was set to zero.

As discussed by *Heelis et al.* [1993], with regard to their investigation into the effects of subauroral ion drifts (SAID) on ion upflows, it is important to understand the effects of the time history of the driver in propelling the ionospheric dynamics. In modeling observed upflow events, *Caton et al.* [1996] and *Liu et al.* [1995] considered the precipitation to have been turned on abruptly at 30 min prior to the time of observation, although an exact time history was not known. Here we have chosen to allow the energy flux to linearly increase from zero to its maximum level over a period of 30 min. The characteristic precipitating electron energy was chosen to remain constant, while the energy flux was linearly increased over the first 30 min, then allowed to continue at this level for the duration of the event. All of the ion results presented here are for the major ion species O^+.

3. Relationship of F Region Ionospheric Parameters to the Soft-Electron Precipitation Characteristics

An analysis of DE 2 observations by *Seo et al.* [1997] found that at approximately 800 km altitude a quasi-inverse relationship is seen between the observed field-aligned ion upflow velocities and fluxes and the characteristic energy of the precipitating soft electrons (<1 keV) for restricted ranges of electron energy flux. To model this effect, the precipitating energy flux was held constant at 1.75 ergs cm^{-2} s^{-1}, while the characteris-

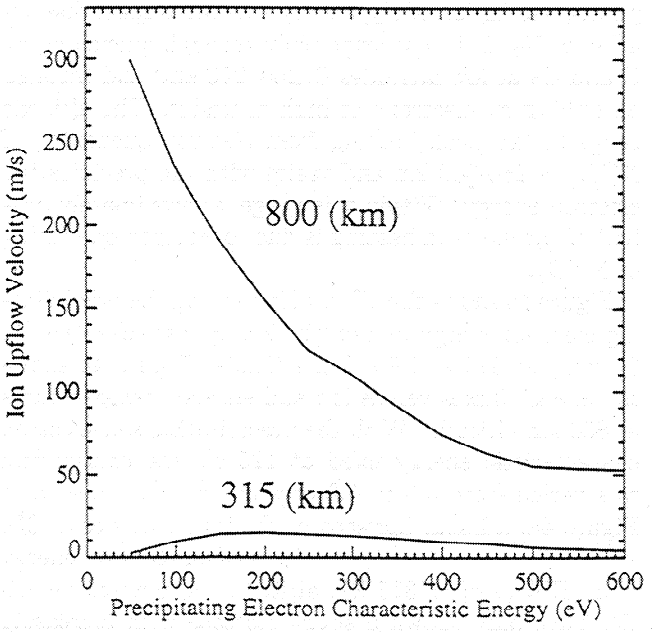

Figure 1a. Modeling results for the ionospheric field-aligned ion velocity at 315 and 800 km altitude versus the characteristic electron precipitation energy from 50 to 600 eV for a fixed precipitation energy flux of 1.75 ergs cm^{-2} s^{-1}.

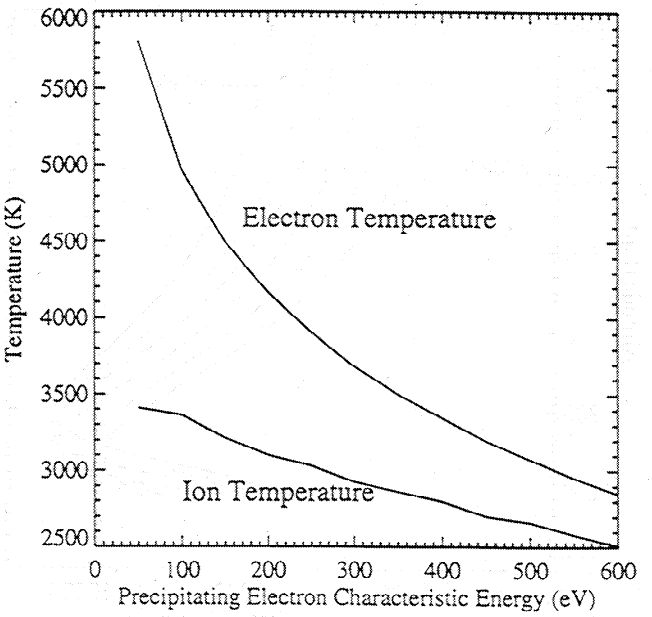

Figure 1b. Ion and electron temperatures at 800 km altitude versus precipitation average energy from 50 to 600 eV for a fixed precipitation energy flux of 1.75 ergs cm^{-2} s^{-1}.

tic energy was varied from 50 to 600 eV for different runs. Each run was sampled after the (ramped) precipitation had been on for 30 min. In Figure 1a the field-aligned ion velocities at 315 and 800 km altitude are plotted versus the characteristic energy of the precipitating electrons. Here it is evident, for the topside regions, that the largest upflow velocities are found at the lowest values of characteristic precipitating electron energy for these runs for which the energy flux was held constant. At 800 km a steady increase in the ion velocity occurs as the characteristic energy is reduced. This trend is attributed at least partially to the fact that more precipitating electrons are available (at constant energy flux) to heat the thermal electrons, thus enhancing the thermal electron temperature (see also Figure 1b) and hence the ambipolar electric field for propelling the upward O^+ flows. Also, for the lower-energy precipitating fluxes their energy is deposited at higher altitudes, where their energy is more efficiently transfered to the ions and electrons. Within the F region at 315 km altitude the velocities increase with increasing energy when the precipitating electron characteristic energy is less than 200 eV and decrease with increasing energy between 200 and 600 eV.

The electron and ion temperatures at 800 km are plotted versus the characteristic energy of the precipitating electrons in Figure 1b. Again, the energy flux was held constant at 1.75 ergs cm^{-2} s^{-1}. The electron temperature, which is significantly higher than the ion temperature, shows a monotonic decrease with increasing characteristic energy. This enhancement of T_e with lowered characteristic energies contributes to an increased ambipolar electric field which propel the upflows as displayed in Figure 1a. The ion temperature shows a very slight increase (compared with the increase seen in the electron temperature) at low characteristic energies of the precipitation. It is evident that the much less responsive ion temperature is still closely tied to the neutral temperatures even at these 800 km altitudes.

Ionospheric electron heating rates at different altitudes are plotted versus the characteristic precipitating

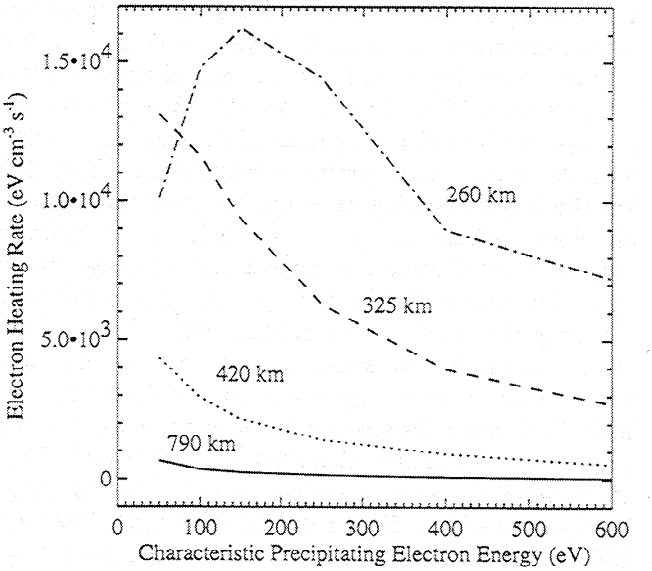

Figure 2. Ionospheric electron heating rate versus characteristic precipitating electron energy from 50 to 600 eV at 260, 325, 420, and 790 km altitudes.

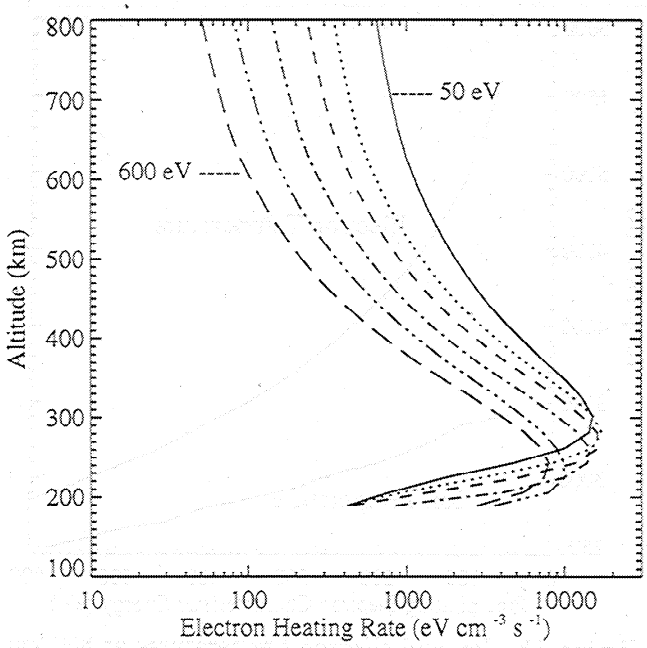

Figure 3. Modeled electron heating rates versus altitude for characteristic precipitation energies ranging from 50 to 600 eV. The solid, dotted, short-dashed, dash-dot-dashed, dash-dot-dot-dot-dashed, and long-dashed lines are for average energies of 50, 100, 150, 250, 400, and 600 eV, respectively.

electron energy from 50 to 600 eV in Figure 2 when the electron precipitation was turned on for 30 min. At altitudes of 325 to 790 km the heating rate monotonically increases with decreasing characteristic energy down to 50 eV, which is consistent with the enhanced electron temperatures seen in Figure 1b. The electron heating rate at 790 km is negligible compared to heating at 325 km. At lower altitudes, for example, 260 km, the peak in the heating rate occurs at a characteristic precipitation energy of about 150 eV. This peak can be understood from Figure 3, which displays the electron heating rate as a function of altitude for several characteristic energies from 50 to 600 eV. At ~250-300 km altitude a crossover is evident in terms of the heating relation with dominant characteristic energy levels. Above 300 km the largest heating rates are produced by the lowest characteristic energy levels, while the opposite is true at lower altitudes. Figures 2 and 3 are associated with Coulomb collisions with primary and secondary electrons produced by the primary auroral precipitating electrons. In that sense, the ultimate thermal electron heating rates at a given altitude are determined by both Coulomb collisions and ionization processes which produce the secondary electrons [cf. *Banks and Nagy*, 1970]. Also, the electron quenching of $N(^2D)$ is a significant source of heat for ionospheric electrons [*Richards*, 1986]. The metastable $N(^2D)$ atom which lies 2.4 eV in energy above the ground state $N(^4S)$ atom is produced in copious quantities in the upper atmosphere by chemical reactions involving NO^+, N_2^+, and N^+, by photodissociation of N_2, and by electron impact dissociation of N_2. It is lost principally through quenching by O and O_2 at low altitudes (below 250 km) and through quenching by electrons at high altitudes. The altitude range of the peak heating from electron quenching of $N(^2D)$ is 250-300 km and varies with the precipitating electron energy. Within this range, approximately one-half of the electron heating is due to electron quenching of $N(^2D)$.

Figure 4a shows the effect of increasing the precipitating electron energy flux on the ion upflow velocities (at 30 min) at 315 and 800 km altitude. Figure 4b shows the energy fluxes versus ion and electron temperatures at 800 km altitude. With the precipitating soft-electron characteristic energy fixed at 125 eV the energy flux was varied from 0.5 to 6.0 ergs cm^{-2} s^{-1}. As seen in Figure 4a, a linear increase in the ion velocities at 800 km altitude results from the increasing electron energy flux. However, at 315 km altitude the upward velocities have only shown a slight increase with increasing energy flux. The plot of the ion and electron temperatures versus electron energy flux (Figure 4b) shows a nearly linear increase in electron temperatures with increasing energy flux at 800 km altitude. The increase seen in the ion temperatures is much smaller. Figures 4a and 4b together illustrate how the ionospheric upflows are driven by the increased ambipolar electric field due to precipitation-enhanced electron temperatures.

Figures 5a and 5b elucidate the variations (at 30 min) of the F region and topside upflow velocities and electron and ion temperatures with characteristic average

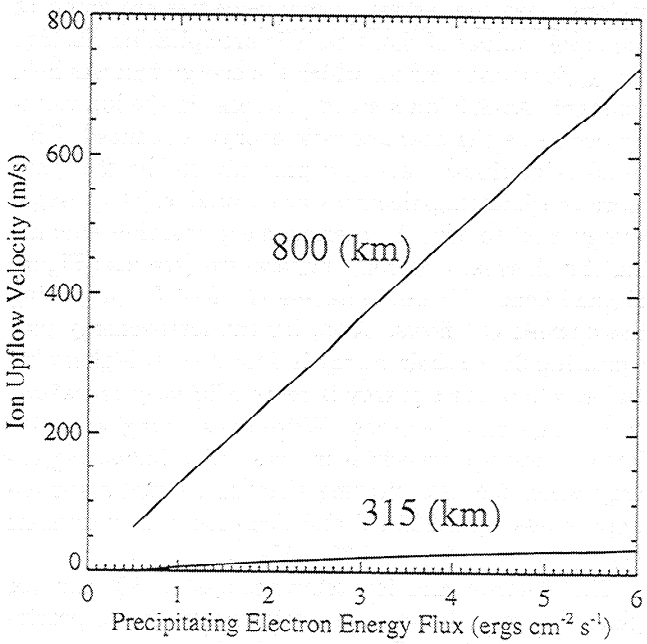

Figure 4a. The modeled field-aligned ion velocities (at 315 and 800 km) plotted versus the precipitating electron energy flux with a constant characteristic precipitating energy of 125 eV. These field-aligned velocities are for 30 min after the electron precipitation turn-on.

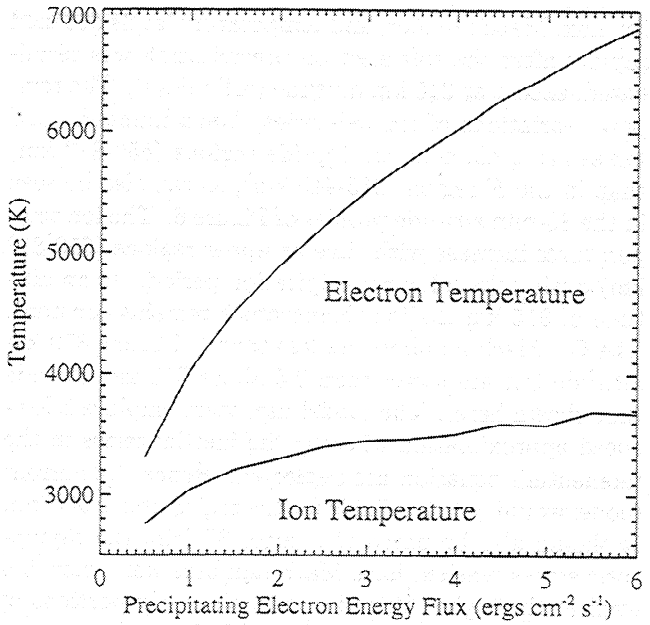

Figure 4b. Complementary to Figure 1b, the ion and electron temperatures at 800 km are here plotted versus the precipitating energy flux with fixed precipitation characteristic energy of 125 eV.

energy again, but this time with the precipitation electron number flux held constant, instead of the energy flux. Figure 5a is a plot of the asymptotic O^+ upflow velocity at 315 and 800 km altitude versus precipitation characteristic energy from 50 to 600 eV (correspondent energy flux from 0.4 to 4.8 ergs cm^{-2} s^{-1}) for a constant precipitating electron number flux of 5×10^9 cm^{-2} s^{-1}. Under these conditions, it is evident that for constant number flux the asymptotic velocity at 800 km altitude rises fairly sharply with the characteristic electron energy, from about 70 to 140 m s^{-1} over the characteristic electron energy range 50 to 150 eV, but then gradually declines for higher energies. The F region upflow velocity similarly rises from 0 to about 20 m s^{-1} for between 100 and about 300 eV and then is fairly level for higher energies. These results tend to support the suggestion that the Figure 1a trend, showing the highest upflow velocities for the lowest precipitating electron characteristic energies for constant electron energy flux, occurs because in that case the number of precipitating electrons available for heating the ionospheric thermal electrons increases as the characteristic energy declines.

Figure 5b shows the electron and ion temperatures at 800 km altitude versus precipitating electron characteristic energy, while holding the precipitating electron number flux constant. Here we see that both the ion and electron topside temperatures are relatively insensitive to the energy of the electrons. Hence we see that the effect of enhanced electron temperatures at low precipitating electron energies displayed in Figure 1b is also, at constant energy flux, the consequence of the increase of the number of precipitating electrons as the characteristic energy decreases.

4. Time Development of Precipitation-Induced Ionospheric Fluxes

In this section we investigate the time development of the ionospheric parameters in response to the ramped turn-on of the precipitation. Both *Liu et al.* [1995] and *Caton et al.* [1996] modeled "snapshots" of spacecraft and radar observations of ionospheric upflow events. However, modeling by *Heelis et al.* [1993] has shown that the upflow velocities for SAID-driven events are sensitive to the timescale of the SAID turn-on. Here the results shown in Figures 6-8 illustrate the temporal response to a precipitation event in order to obtain a better understanding of the time history of the upflow characteristics in precipitation-driven events.

For the case examined here, the precipitation is turned on at 2130 UT and allowed to continue for 2 hours, again at the latitude and longitude corresponding to the EISCAT radar facility. For Figures 6 and 7 the characteristic energy was held constant (125 eV), while the electron energy flux was linearly increased over the first 30 min and then allowed to remain at the maximum level for 1.5 hours before being shut off. Figure 6 shows the ion velocities (Figure 6a) and fluxes (Figure 6b) along the flux tube from 200 to 1000 km, where the leftmost solid line in each panel corresponds to conditions at 1.2 min before the time of the precipitation turn-on. Figure 7 shows the ion upflow velocities (Figure 7a), fluxes (Figure 7b), Mach numbers (Figure 7c), and temperatures (Figure 7d) versus time from the on-

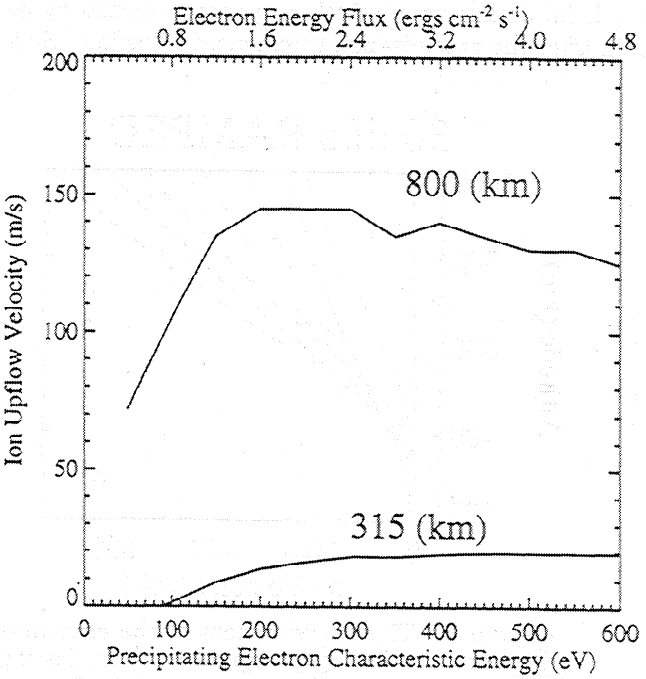

Figure 5a. The modeled field-aligned ion velocities (at 315 and 800 km) plotted versus the characteristic precipitating electron energy flux with a constant characteristic precipitating number flux of 5×10^9 cm^{-2} s^{-1}. These field-aligned velocities are for 30 min after the electron precipitation turn-on.

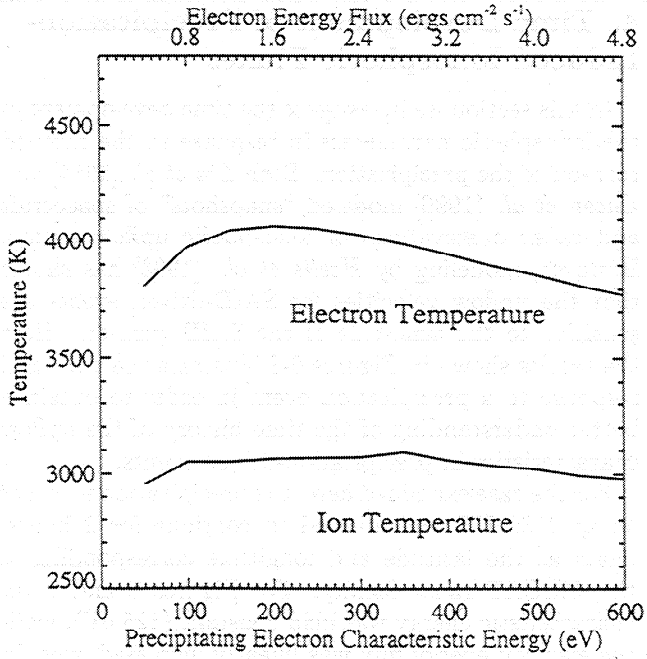

Figure 5b. Complementary to Figure 4b, the ion and electron temperatures at 800 km are here plotted versus the precipitating characteristic energy flux for constant precipitation number flux of 5×10^9 cm^{-2} s^{-1}.

set of the precipitation. The definition of Mach number used in this paper is the parallel flow speed divided by the ion thermal speed, as was used by *Seo et al.* [1997].

As can be seen, the maximum velocity, Mach number, and flux were attained at 10-13 min, followed by a partial decline to relatively constant velocities by 30 min after the precipitation commenced. The ion velocity, flux, Mach number, and temperature levels declined rapidly after the soft-electron precipitation was terminated, except at 315 km altitude (solid lines). The temporal variations of ion velocities, Mach numbers, and fluxes are greater in the topside regions (650-810 km) than in the F region (315-440 km), as can also be seen in the 30-min altitude profiles of Figure 6. The ion temperatures increase with time at upper regions (650-810 km) during the 2-hour precipitation period. At an altitude of 315 km the ion temperature remains constant. The O^+ Mach numbers are less than 0.4 below 810 km altitude but are larger than 0.5 above 950 km altitude (not shown here). The model used here employs a low-speed approximation whereby the inertial terms in the momentum equation are neglected. Hence the current model would not be reliable for the region above 950 km. It should also be noted that after 30 min, the asymptotic states reached have Mach numbers well below 0.4 even at the higher altitudes; only the early portions of the temporal developments have Mach numbers above 0.4 at the higher altitudes. It is the parameters for 30 min after precipitation turn-on which constitute the focus of the cases in Figures 1-5.

We have also examined the electron temperatures (Figure 8a) and Mach number for H^+ ions (Figure 8b), where the line legend is same as that in Figure 7. The electron temperature increased dramatically in the first 30 min at all altitudes, then remained nearly constant until the precipitation was turned off. The H^+ Mach numbers are less than 0.15 below 810 km altitude, which also validates the model for the minority species.

The different time periods for increasing the electron energy flux to the maximum have also been examined.

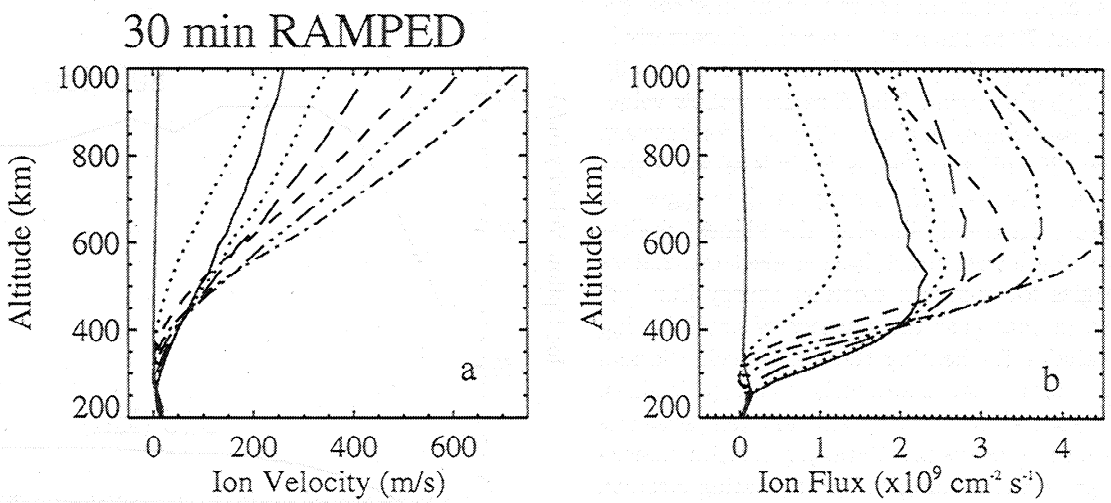

Figure 6. Time development of the altitudinal profiles for (a) ion field-aligned velocities and (b) fluxes created by precipitation event lasting 2 hours with an ramped (linearly over 30 min) turn-on of the precipitation energy flux. The characteristic precipitating electron energy was 125 eV, while the maximum energy flux was 1.0 ergs cm^{-2} s^{-1}. The leftmost solid line in each plot corresponds to conditions at 1.2 minutes before the time of the precipitation turn-on. The line legends are leftmost solid line, -1.2 min; leftmost dotted line, 3 min; short dashed line, 7.2 min; dash-dot-dashed line, 10.8 min; dash-dot-dot-dot-dashed line, 15 min; long dashed line, 21 min; second (rightmost) dotted line, 28.2 min; second (rightmost) solid line, 32.4 min.

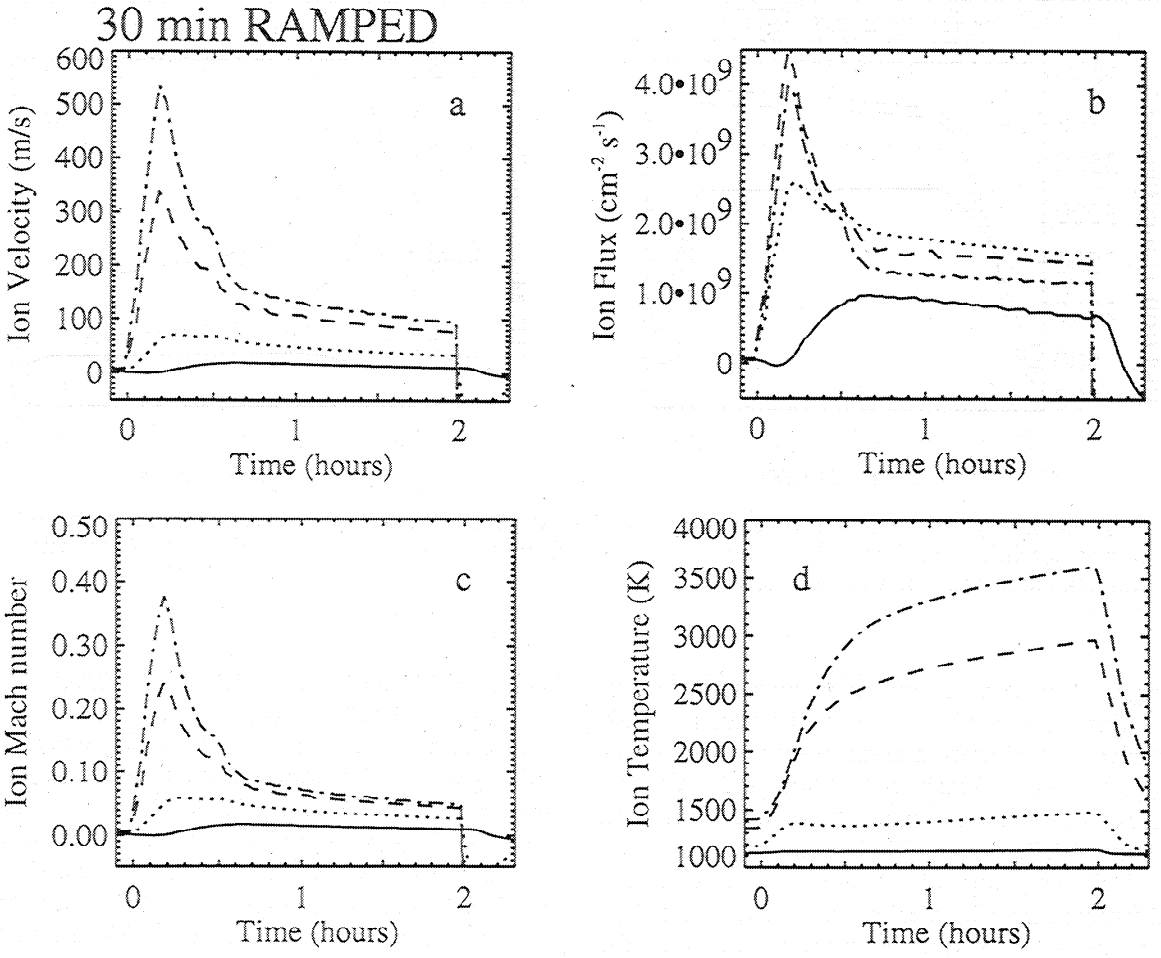

Figure 7. (a) Ion upflow velocities, (b) fluxes, (c) Mach numbers, and (d) temperature, again for the ramped turn-on of the precipitation, here plotted versus the time from the onset of the precipitation and shown for altitudes of 315 km (solid line), 440 km (dotted line), 650 km (dashed line), and 810 km (dash-dot-dashed line).

We have found that the peak ion upward velocity attains to a higher value, when the "ramping" precipitation time is short, which is similar to the SAID-driven events by *Heelis et al.* [1993]. However, similar velocity profiles are achieved with either of the ramping conditions. In each case, a nearly constant velocity was reached after 30 min after the precipitation onset. For the cases in Figures 1-5 the ion Mach numbers are less than 0.4 after the first 30 min, which tend to validate the use of low-speed-approximation model.

5. Discussion

The modeling results reported here are qualitatively consistent with several trends found from recent statistical analysis of topside ionospheric characteristics of upflows observed with the DE 2 spacecraft from seven auroral zone passes in the evening sector [*Seo et al.*, 1997]. Those observations were for the topside altitude range 850-950 km.

Seo et al. [1997], for example, found that the observed ion field-aligned upflow velocities were strongly correlated with electron temperatures. The characteristic correlation coefficient for the upflow velocities observed was r=0.97 with the (binned, averaged) electron temperatures T_e. They were less well correlated, r=0.4, with the ion temperatures T_i. This is consistent with the notion that the thermal electron heating, such as through the soft-electron precipitation effects described here, is more influential on the ion upflows than the ion heating due to convection-driven friction.

Further consistency with the DE 2 observations is seen by noting that *Seo et al.* [1997] found, in examining the upflows in restricted ranges of energy flux, that the largest velocities were observed when the average soft-electron energies were below 100 eV. In terms of fluxes, *Seo et al.* [1997] reported upward fluxes only exceeding 5×10^9 ions cm^{-2} s^{-1} for electron average energies below 100 eV and unusually large fluxes exceeding 10^{10} ions cm^{-2} s^{-1} for electron average energies below 50 eV.

In addition, *Seo et al* [1997] found that when the DE 2 topside data were binned in narrow ranges of plasma density and precipitating soft-electron energy flux, the electron temperatures decline with the aver-

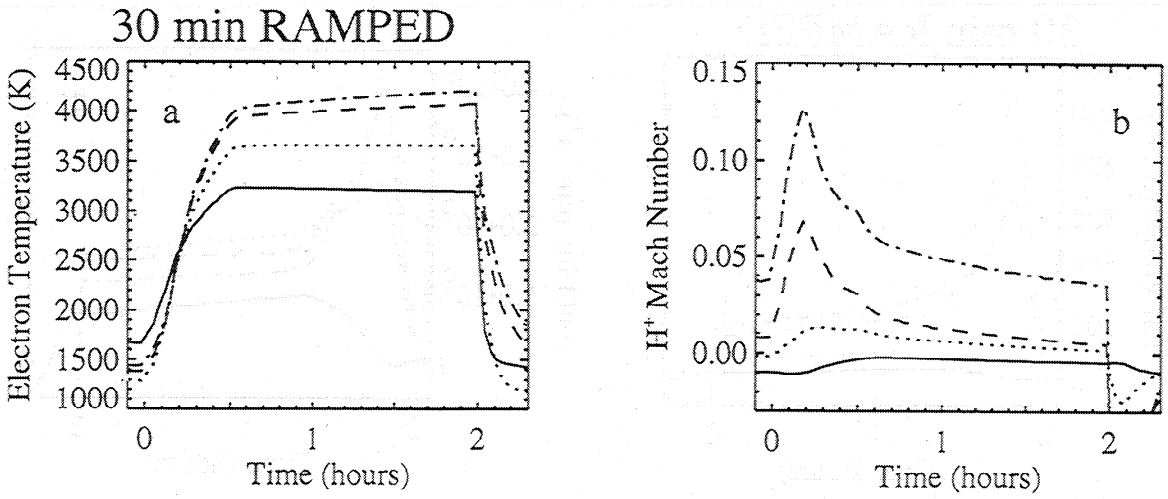

Figure 8. (a) Electron temperatures and (b) H^+ Mach numbers again for the ramped turn-on of the precipitation, here plotted versus the time from the onset of the precipitation, where the line legend is same as that in Figure 7.

age energy, as was seen in our modeling results in Figure 1b. Their observed T_e fit a linear decrease with (bin-averaged) precipitation average energy with a correlation coefficient coefficient of $r = -0.9$. On the other hand, the electron temperature values observed by *Seo et al.* [1997] were significantly lower, in the range 2000-4000 K, than those of the modeling in Figure 1b. Such differences may be attributed to magnetospheric heat flux assumptions and neutral atmospheric model values. *Seo et al.* [1997] also examined the observed ion temperature variation with average energy and observed linear decrease, with a correlation coefficient of $r = -0.89$; however, the slope was not quite as steep when compared to that of the electron temperature. Such observed trends are again qualitatively consistent with the slight decline of the ion temperature with average energy seen here in our model results (Figure 1b). Furthermore, *Seo et al.* [1997] showed that T_e and T_i displayed increasing trends with precipitating electron energy flux when the data were binned in narrow ranges of average energy, as might also be expected if the soft-electron precipitation is indeed responsible for much of the topside electron temperature variation at topside altitudes, and in agreement with the modeled variations here as shown in Figure 4b.

We also note that *Seo et al.* [1997] examined the field-aligned O^+ ion Mach numbers observed by DE 2 between 850 and 950 km altitude. They found that the Mach numbers were typically below 0.4 for the data they examined. *Seo et al.* [1997] also found that these ion Mach numbers were strongly correlated with local T_e. Our model results also indicate Mach numbers of this order in the corresponding altitude ranges (Figure 7). Since we have found that Mach numbers above 900 km (not shown) are larger in some instances, it is possible some of the below 800 km results may be compromised (in this FLIP/low-speed approximation treatment) by the large upflow velocities at the higher altitude (>950 km).

Since the FLIP code involves a low-speed approximation, we checked its validity for the present study by examining results for comparable conditions from the FLIP code with results from a case using a newly developed dynamic fluid-kinetic (DyFK) model [*Estep et al.*, 1998; *Wu et al.*, 1998], which combines the fluid treatment for the ionosphere (up to 800 km) and a semiki-

Table 1. Mach Number Comparison

Altitude, km	FLIP M_{O^+}	DyFK M_{O^+}	FLIP M_{H^+}	DyFK M_{H^+}
310	0.047	0.043	0.019	0.013
400	0.15	0.12	0.05	0.03
513	0.24	0.18	0.06	0.04
610	0.27	0.20	0.10	0.06
725	0.30	0.23	0.19	0.12
813	0.31	0.27	0.26	0.18
915	0.33	0.31	0.33	0.31
1025	0.35	0.32	0.46	0.32

M, Mach number; DyFK, dynamic fluid-kinetic model.

netic treatment for high altitudes. This new code takes much longer to ran than the FLIP code, but since the 800-km kinetic portion has no low-speed approximation involved, it is a accurate for all altitudes and has been tested under various conditions. Thus it is a suitable comparison for addressing whether the Mach numbers and general behaviors for the FLIP results in this paper are reasonably accurate. The precipitation characteristic energy in this comparison case was taken to be 100 eV, and the energy flux was 3 erg cm^{-2} s^{-1} at 800 km. After precipitation turn-on for about 30 min the O^+ and H^+ Mach numbers from the DyFK mo iel and from the FLIP model are listed in Table 1. The Mach numbers are higher from the FLIP model than from the DyFK model. The O^+ Mach numbers from the DyFK model are thus seen to be in aggreement by 6-30% with the results from the FLIP model while the H^+ Mach numbers are seen to be in agreement within 6-40%. The high-speed result at high altitude does influence the result at low altitude in FLIP slightly, but it does not change the physics phenomena presented in this paper. Hence we generally expect that the results in the present FLIP modeling of the soft-electron precipitation effects on the F region/topside ionosphere to be in fact representative for the 300-800 km altitude results explored here.

In Figure 9 we display the ambipolar electric field profiles to demonstrate how soft-electron precipitation can affect ionospheric ion upflows through enhancement of this ambipolar electric field. The ambipolar electric field, which is proportional to both the density and temperature gradients, may be expressed as

$$E_{||} = -\frac{k}{e}(1+\frac{\alpha}{2})\nabla T_e(r) - \frac{kT_e}{eN_e(r)}\nabla N_e(r) \quad (1)$$

where k is the Boltzmann constant, e is electron charge, T_e is electron temperature (a function of altitude r), N_e is the electron density, and α is the thermal diffusion coefficient. The flow of plasma is critically determined by the sign of the electric field. For the ordinary polar wind, $E_{||}$ is generally positive. For negative $E_{||}$, the upflow is hindered. The developing altitudinal profiles for

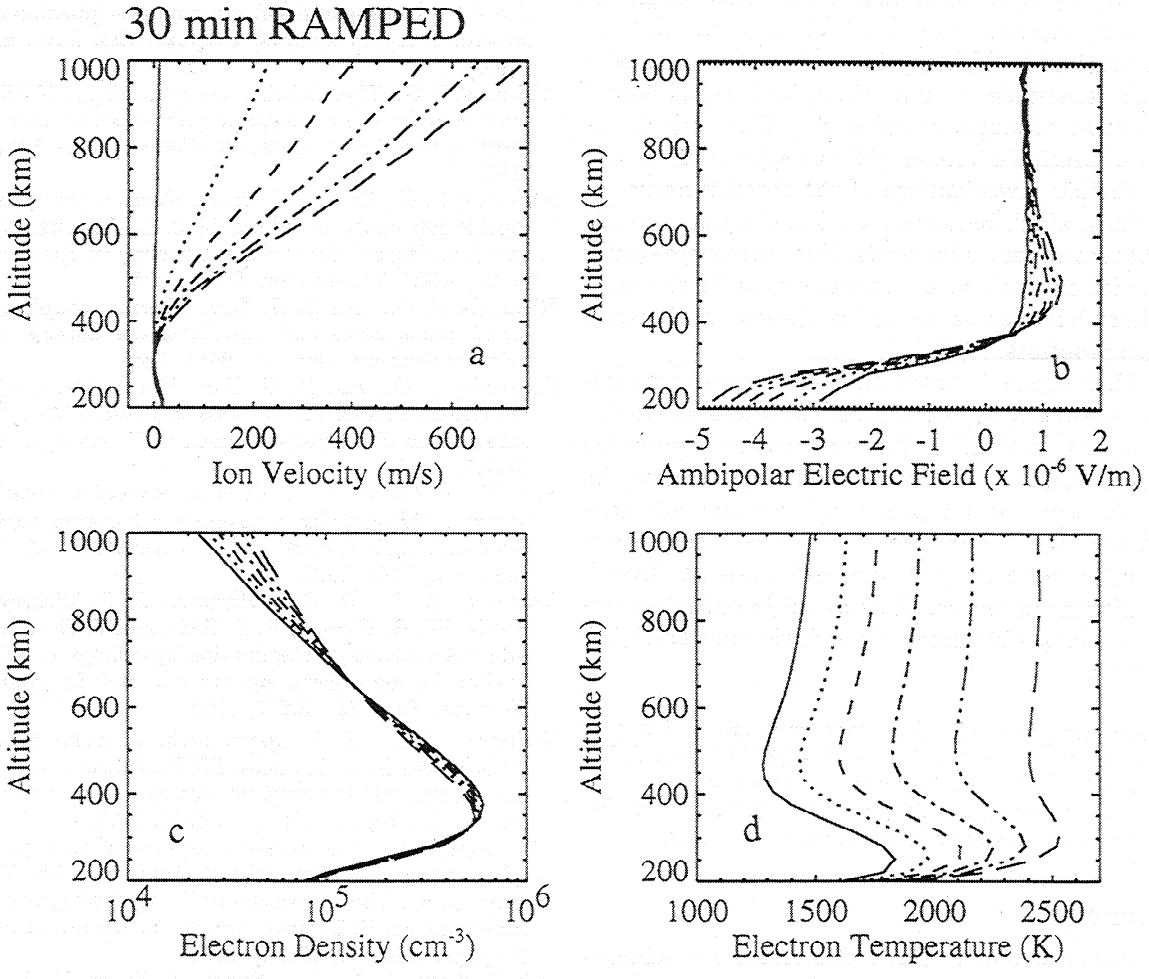

Figure 9. Time development of the altitudinal profiles for (a) ion field-aligned velocities, (b) ambipolar electric field, (c) electron densities, and (d) electron temperatures. The conditions are the same as in Figures 6-8. The line legends are solid line, -1.2 min; dotted line, 3 min; short dashed line, 4.8 min; dash-dot-dashed line, 7.2 min; dash-dot-dot-dot-dashed line, 9 min; long dashed line, 10.8 min.

ion field-aligned velocities (Figure 9a), ambipolar electric field (Figure 9b), electron densities (Figure 9c), and electron temperatures (Figure 9d) are shown in Figure 9 for the same conditions as in Figure 7. Figure 9 shows that the rapidly increasing electron temperature during the first 11 min increased the ambipolar electric field and propelled the upward O^+ flows. One way to look at this situation is that the ions would gain a flow energy from the associated ambipolar electron of about 0.3 eV over 300 km from the 1 μV m^{-}1 electric field. This flow energy would correspond to about 1 km s^{-1}, which is comparable to the peak flow velocity at the upper altitude ranges. By 30 min after the precipitation turn-on, the electron temperatures tend to stabilize, and then the ion velocities and fluxes attained the nearly constant values (see Figure 7).

Recent studies (e.g., reviewed by *Daglis and Axford* [1996]) have indicated a fast and effective feeding of the magnetosphere with energetic ionospheric origin ions during periods of enhanced auroral electrojects, i.e., during the expansion and the late growth phase of substorms. *Daglis and Axford* [1996] suggested that a fast feeding (of the order of 10 min) of the near magnetotail with ionospheric ions can lead to a transient localized dominance of heavy ionospheric ions (namely, O^+) and, consequently, to an ionospheric regulation of the evolution of magnetic substorm. Our time development of precipitation-induced ionospheric fluxes will help in further investigations of the detailed nature of O^+ outflow, which becomes a critical element at times of intense storms and substorms. The ionosphere should be regarded not only as a material source for the magnetosphere but also as an active element in dynamic geospace processes.

The FLIP model is based on the low-speed approximation, which may break down for altitudes above 800 km on auroral field lines. We are currently developing a DyFK model to combine the fluid treatment for the ionosphere and a semikinetic model for high altitudes [e.g., *Estep et al.*, 1998; *Wu et al.*, 1998]. This model should allow more complete and self-consistent investigation of upflows and outflows as subjected to various auroral processes including the soft electron precipitation effects.

Acknowledgments. This work was supported in part by NSF grants ATM-9402310, ATM-9523786, and ATM-9612573 to University of Alabama in Huntsville.

Janet G. Luhmann thanks Ionnis A. Daglis and another referee for their assistance in evaluating this paper.

References

Banks, P. M., and A. F. Nagy, Concerning the influence of elastic scattering upon photoelectron transport and escape, *J. Geophys. Res., 75,* 1902, 1970.

Caton, R., J. L. Horwitz, P. G. Richards, and C. Liu, Modeling of F-region ionospheric upflows observed by EISCAT, *Geophys. Res. Lett., 23,* 1537, 1996.

Daglis, I. A., and W. I. Axford, Fast ionospheric response to enhanced activity in geospace: Ion feeding of the inner magnetotail, *J. Geophys. Res., 101,* 5047, 1996.

Estep, G. M., Y.-J. Su, J. L. Horwitz, P. G. Richards, G. R. Wilson, and D. G. Brown, A dynamics coupled fluid-semikinetic model for ionosphere-magnetosphere plasma transport: Effects of ionization by soft electron precipitation, *Eos Trans. AGU, 79*(17), Spring Meet. Suppl., S317, 1998.

Ganguli, G., M. J. Keskinen, H. Romero, R. Heelis, T. E. Moore, and C. J. Pollock, Coupling of microprocesses and macroprocesses due to velocity shear: An application to the low-altitude ionosphere, *J. Geophys. Res., 99,* 8873, 1994.

Hedin, A. E., MSIS-86 thermosphere model, *J. Geophys. Res., 92,* 4649, 1987.

Hedin, A. E., et al., Revised global model of thermospheric winds using satellite and ground-based observations, *J. Geophys. Res., 96,* 7657, 1991.

Heelis, R. A., G. J. Bailey, R. Sellek, R. J. Moffett, and B. Jenkins, Field-aligned drifts in subauroral ion drift events, *J. Geophys. Res., 98,* 21,493, 1993.

Korosmezey, A., C. E. Rasmussen, T. I. Gombosi, and G. V. Khazanov, Anisotropic ion heating and parallel O^+ acceleration in regions of rapid ExB convection, *Geophys. Res. Lett., 19,* 2289, 1992.

Liu, C., J. L. Horwitz, and P. G. Richards, Effects of frictional ion heating and soft-electron precipitation on high-latitude F-region upflows, *Geophys. Res. Lett., 22,* 2713, 1995.

Richards, P. G., Thermal electron quenching of $N(^2D)$: Consequences for the ionospheric photoelectron flux and the thermal electron temperature, *Planet. Space Sci., 8,* 689, 1986.

Richards, P. G., Effects of auroral electron precipitation on topside ion outflows, edited by J. L. Horwitz, N. Singh, and J. L. Burch, *Cross-Scale Coupling in Space Plasmas,* p.121, AGU, Washington, D.C., 1995.

Richards, P. G., and D. G. Torr, Thermal coupling of conjugate ionospheres and the tilt of the Earth's magnetic field, *J. Geophys. Res., 91,* 9017, 1986.

Richards, P. G., and D. G. Torr, Theoretical modeling of the dependence of the N_2 second positive 3371 Åautotal emission on characteristic energy, *J. Geophys. Res., 95,* 10,337, 1990.

Seo, Y., R. Caton, J. L. Horwitz, Statistical relationships between high-latitude ionosphyeric F-region/topside upflows and their drivers: DE-2 observations, *J. Geophys. Res., 102,* 7493, 1997.

Tsunoda, R. T., R. C. Livingston, J. F. Vickrey, R. A. Heelis, W. B. Hanson, F. J. Rich, and P. Bythrow, Day-side observations of thermal-ion upwellings at 800 km altitude: An ionospheric signature of cleft ion fountain, *J. Geophys. Res., 94,* 15,277, 1989.

Wahlund, J.-E., H. J. Opgenoorth, I. Haggstrom, K. J. Winser, and G. O. L. Jones, EISCAT observations of topside ionospheric ion outflows during auroral activity: Revisited, *J. Geophys. Res., 97,* 3019, 1992.

Whitteker, J. H., The transient response of the topside ionosphere to precipitation, *Planet. Space Sci., 25,* 773, 1977.

Wilson, G. R., The generation of O^+ upflowing velocity distributions via ExB convection in the transition region, *J. Geophys. Res., 99,* 17,453, 1994.

Winningham, J. D., J. L. Burch, N. Eaker, V. A. Blevins, and R. A. Hoffman, The low-altitude plasma intrument (LAPI), *Space Sci. Instrum., 5,* 465, 1981.

Wu, X.-Y., J. L. Horwitz, G. M. Estep, Y.-J. Su, D. G. Brown, P. G. Richards, and G. R. Wilson, Dynamic fluid

kinetic (DyFK) modeling of auroral plasma outflow driven by soft electron precipitation and transverse ion heating, *J. Geophys. Res.*, in review, 1998.

Yeh, H.-C., and J. C. Foster, Storm-time heavy ion outflow at mid-latitude, *J. Geophys. Res., 95,* 7881, 1990.

R. G. Caton, Radex Inc., #3 Preston Ct., Bedford, MA 01730. (e-mail: caton@ziggy.radex.plh.af.mil)

J. L. Horwitz and P. G. Richards, Center for Space Plasma and Aeronomic Research, The University of Alabama in Huntsville, Huntsville, AL 35899. (e-mail: horwitzj@cspar.uah.edu; richards@cs.uah.edu)

Y.-J. Su, Space and Atmospheric Sciences, NIS-1, MS D466, Los Alamos National Laboratory, Los Alamos, NM 87545. (e-mail: ysu@lanl.gov)

(Received November 25, 1997; revised September 17, 1998; accepted October 14, 1998.)